BEILSTEIN ARCHIVES

This open access document is posted as a preprint in the Beilstein Archives at https://doi.org/10.3762/bxiv.2024.67.v1 and is considered to be an early communication for feedback before peer review. Before citing this document, please check if a final, peer-reviewed version has been published.

This document is not formatted, has not undergone copyediting or typesetting, and may contain errors, unsubstantiated scientific claims or preliminary data.

Preprint Title	Performance optimization of microwave-coupled plasma-based ultra-low energy ECR ion source for silicon nano-structuring and application
Authors	Joy Mukherjee, Safiul A. Mullick, Tanmoy Basu and Tapobrata Som
Publication Date	22 Nov. 2024
Article Type	Full Research Paper
ORCID® iDs	Joy Mukherjee - https://orcid.org/0000-0002-5387-2617; Safiul A. Mullick - https://orcid.org/0000-0002-0985-8914

License and Terms: This document is copyright 2024 the Author(s); licensee Beilstein-Institut.

This is an open access work under the terms of the Creative Commons Attribution License (https://creativecommons.org/licenses/by/4.0). Please note that the reuse, redistribution and reproduction in particular requires that the author(s) and source are credited and that individual graphics may be subject to special legal provisions.
The license is subject to the Beilstein Archives terms and conditions: https://www.beilstein-archives.org/xiv/terms.
The definitive version of this work can be found at https://doi.org/10.3762/bxiv.2024.67.v1

Performance optimization of microwave-coupled plasma-based ultra-low energy ECR ion source for silicon nano-structuring and application

Joy Mukherjee[1], Safiul Alam Mullick[2], Tanmoy Basu[3], Tapobrata Som[1,4*]

[1]SUNAG Laboratory, Institute of Physics, HBNI, Sachivalaya Marg, Bhubaneswar – 751 005, India

[2]Rabindra Mahavidyalaya, University of Burdwan, Hooghly, West Bengal, 712 401

[3]Centre for Quantum Engineering, Research and Education, TCG Centers for Research and Education in Science and Technology, Kolkata, West Bengal, 700 091, India

[4]Homi Bhabha National Institute, Training School Complex, Anushaktinagar, Mumbai – 400 085, India

Abstract:

This literature presents a comprehensive optimization of key parameters crucial for generating ion beams in a microwave-coupled plasma-based ultra-low energy Electron Cyclotron Resonance (ECR) ion source, generally used for nano-structuring on solid surfaces. The investigation focuses on developing, accelerating, and extracting Ar^+ ions from a magnetron (microwave) coupled plasma cup utilizing three-grid ion extraction composed of molybdenum. The study systematically examines the dependence of ion beam current on critical parameters, such as gas pressure, magnetron power, extraction voltage, and ion energies. Additionally, the influence of extraction voltage on beam current is investigated for different ion energies. The variation of beam current as a function of ion energy is explored under constant magnetron current and extraction voltage at various conditions. The Gaussian nature of the beam profile is scrutinized and elucidated within the context of grid extraction-based ion sources. Plasma physics principles are employed to interpret the observed variations in ion current density (beam current) with various parameters. The corresponding ion-induced nanopatterning on silicon, using the optimized beam current, is explored in detail. Furthermore, the research delves into the temporal evolution of the surface topography of silicon followed by off-normal incidences (60º and 72.5º) is Ar-ion extracted at 450 eV Ar-ions. The changes in the optical property, resulting from nano-patterned surfaces, investigated using UV-VIS spectroscopy, is correlated the with dimension of nano patterning. This manuscript highlights the potential applications arising from these findings, emphasizing the transformative impact of low energy inert ion induced nano-patterning technologies.

Keywords: Ultra-low energy ECR-based ion source, Optimization of ion current, Surface topography, TEM, UV-VIS spectroscopy

*Corresponding author email: tsomiop@gmail.com

Introduction:

The ion source serves as a fundamental component in numerous scientific and industrial applications, playing a crucial role in generating charged particles (ions). Following ion production, various systems harness these energetic ions for diverse purposes, spanning material science, high-energy physics, medical applications, and agricultural science[1–5]. Presently, energetic ions find application in various surface treatments such as nano-patterning, sputter etching, controlled defect formation, and more[6,7]. Particularly, ultra-low energy ion beam proves exceptionally valuable for the precise modification of 2D layers [8], ion-induced nano-patterning on semiconductor surfaces[9]. Over the past few decades, ion-induced nano-patterning and nanoscale functionalizations have garnered significant interest, owing to their broad applications in DNA origami [10], tuning wettability [11], electrical and magnetic anisotropy [12,13], isolated dot formation [14], nanoscale plasmonic array[15], field emission [16], etc. Thus, the ion sources generate enormous possibilities for material modifications both physically and chemically. Further, diversity exists in energetic ion production mechanisms. The fundamental process of producing ions is the collision of atoms with ions or electrons which may be either elastic or inelastic. In elastic collisions, the internal energy of the colliding particles does not change. Ionization, stripping, electron capture, and excitation of atoms due to collisions are examples of inelastic collisions. The free electrons colliding with atoms also produce ions. Electrons in the gas are heated by the inductively coupled method and then acquire enough energy to generate plasma. Due to several drawbacks in such Townsend discharge, these sources are not used now a days. In recent days, compact broad-beam ion sources are widely used in scientific laboratories to generate ions. Depending upon the mechanism of production of various ions using gaseous plasma, the ion sources can be classified in three ways; direct current (dc) operated ion sources, radio frequency (microwave) ion sources, and microwave ion sources. In the past few decades, DC ion sources were commonly used in the above activities [17–19]. These DC ion sources consist of a hot cathode or filament, which is not especially useful in cases of reactive gas discharge; hence, their lifetime is limited [20,21]. Moreover, the beam current produced by those ion sources is not suitable for modern-day applications. In material science as well as surface science applications, the ion source should be mobile and adaptable to the vacuum system, having a longer lifetime. Further, the ion source should produce a relatively high beam current (i.e., capable of forming a high density of plasma) with lower maintenance. To address this challenge, Electron Cyclotron Resonance (ECR) based ion sources were developed [22,23]. ECR ion source is one of the most preferred ion sources for the easy production of ions for different energies and charge states. Since the discharge is maintained in the quartz cup via a strong electric field generated in the cavity, the ECR-based ion sources equipped with microwave cavities neither contain any filament nor any type of electrode. The high plasma density within a quartz cup is confined by solenoid magnets surrounding it, creating a multi-cusp magnetic field. However, careful attention is required for the microwave coupling to the plasma cup to minimize microwave-reflected power. Mechanical adjustments to the resonator length and waveguide are made to ensure minimal reflection of microwave power. Additionally, maintaining the necessary magnetic field strength is crucial for sustaining the plasma. The ion source's compact design is user-friendly and capable of producing a high beam current density for a single or multi-grid extraction system. As a result, the extracted beam current is influenced by magnetron power, plasma pressure, and extraction voltage. Furthermore, the beam current varies with different ion energies.

This article focuses on optimizing the beam current generated by a cost-effective microwave-based Electron Cyclotron Resonance (ECR) ion source and subsequent development of nanoscale patterns on the surface of silicon. The relationship between the beam current and various parameters is extensively examined and elucidated. Experimental parameters, spanning from plasma generation to ion beam extraction, are systematically optimized for the study of low-energy Ar-ion-induced nanostructures on silicon. The dependence of the extracted ion beam on plasma pressure, magnetron power, and extraction grid voltage is documented for different ion energies. Additionally, the manuscript establishes the relationship between ion beam current and the ion energy. Irradiation of p-type single crystal Si (100) surface at off-normal angles (60º and 72.5º) by a 450 eV Ar-ion results in the well-defined formation of nanoscale ripple patterns. The prominence of ripple structures increases with prolonged irradiation time, while bombardment at 72.5º with the same ion beam parameters leads to the coarsening of nanostructures. Cross-sectional transmission electron microscopy (TEM) measurements confirm the formation of nanostructure as observed from atomic force microscopy images (AFM). The thickness of the amorphous thin layer is well agreement with Monte Carlo Simulation (SRIM)[24]. The article further investigates and explains the optical response (by UV-VIS spectrophotometer) of the nano-patterned surfaces with the dimensions of nano-patterning (i.e., wavelength and rms roughness). The potential applications of such nano-patterned silicon surfaces are enlightened. This article underscores the versatility of an optimized broad-beam ultra-low energy ion source, specifically in the context of optimization of inert Ar-ion and subsequent ion-induced silicon nano-patterning.

Description of the ion source:

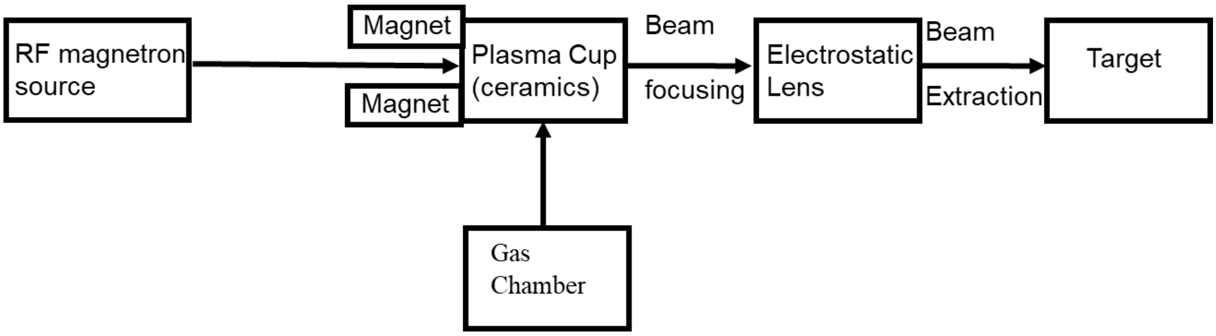

Figure 1: Block diagram consisting of the component of high vacuum plasma ion source equipped with UHV chamber.

Figure 1 illustrates the block diagram of the magnetron-coupled ultra-low energy Electron Cyclotron Resonance (ECR) ion source to provide a comprehensive visualization of the entire setup. The schematic representation in Figure. 1 elucidates the process of extracting an ultra-low energy ion beam. An microwave source (magnetron) is connected to the ceramic plasma cup via a waveguide. The gas inlet system facilitates the filling of the plasma cup with gas through a capillary tube. The intense electric field generated by the microwave source (magnetron) induces gas breakdown (discharge), leading to the formation of a highly intense plasma. The produced plasma is confined and sustained by a permanent magnet positioned near the ceramic plasma cup (made of Al_2O_3). For the extraction and focusing of the beam, a gridded electrostatic lens, commonly referred to as an Einzel lens, is employed. The shape and size of the beam are contingent on the extraction voltage applied at the grid and the corresponding ion energy. The directed beam impacts the silicon target kept in an ultra-high vacuum (UHV) within the target chamber. A faraday cup, connected to a multimeter, measures the beam current, and the corresponding ion fluence is expressed in terms of irradiation time.

The sample holder, located in a UHV chamber, is connected to a 5-axes (x, y, z, θ, φ) manipulator system, offering movement and rotation in all possible directions. The sample is transferred to the ion source using a load-lock system. A later discussion provides a cross-sectional view of the system.

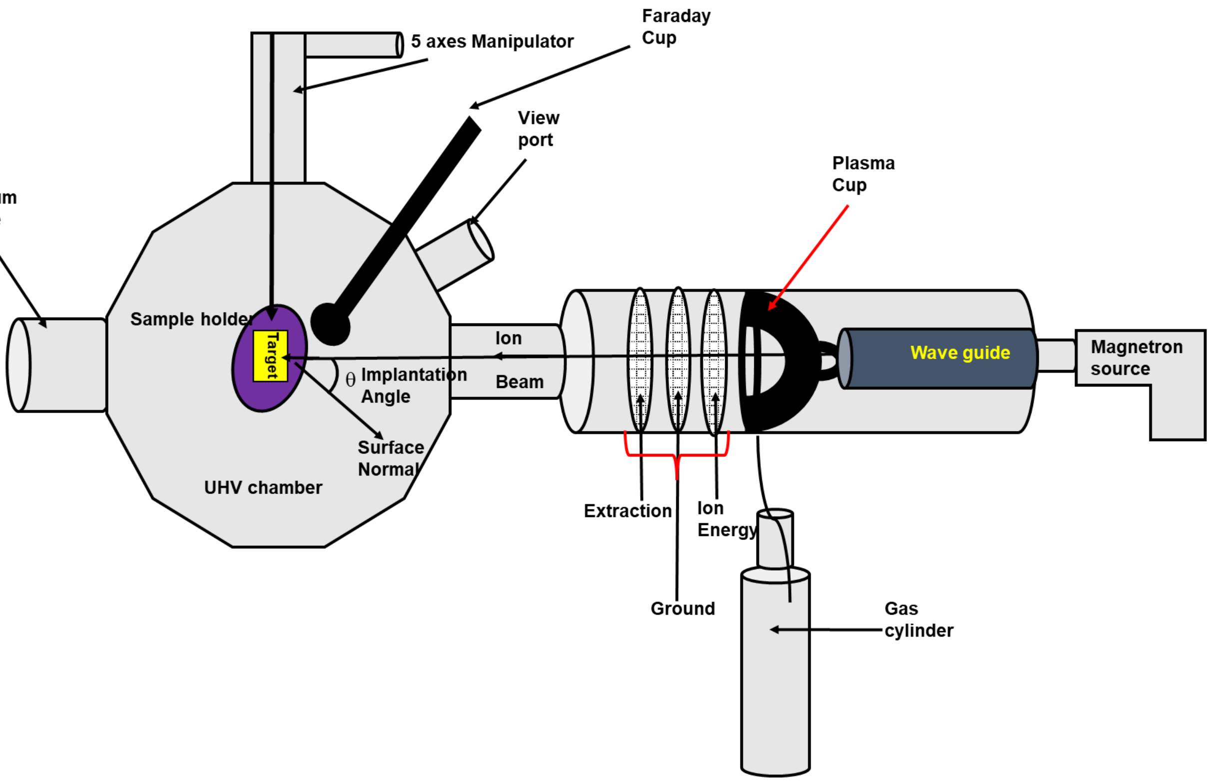

Figure 2: Cross-sectional (schematic) view of microwave coupled ultra-low energy ion beam system.

The cross-sectional view of the high vacuum microwave based ECR ion source mentioned above is shown in Figure 2. The entire system consists of a magnetron-coupled ion source, a UHV target chamber with a cylindrical cavity and load lock, a 5-axes manipulator (PREVAC Technologies), and a gas inlet system. This type of magnetron-coupled ion source was first developed by Anton *et.al* [23]. The ion source is fitted in the cylindrical cavity of the UHV target chamber. The inner diameter of the plasma cup is around 52 mm, where the plasma is generated. The cup is surrounded by water-cooled magnets made up of neodymium-iron-boron, which produces a multi-cusp field to confine the plasma. The 2.45 GHz magnetron-based microwave source is attached to the backside of the ion source, as shown in Figure 2. The dimension of the cylindrical resonator (waveguide) is chosen in such a way that it can produce maximum beam current. To generate plasma in the ceramic cup (known as plasma cup), a gas is inserted into it through a capillary tube attached to the gas chamber. A pressure of 10^{-4} mbar is maintained for sustaining plasma by adjusting a needle valve attached to the gas chamber. The entire length of the ion source is around 130 cm. The extraction of ion beams is accomplished by a three-grid ion optics system, as seen in Figure 2. Wide-ranging extraction voltage is applied to the grid to enable the extraction of an intense beam with different diameters. The circular perfection of the beam shape is evident from observations on the front plate attached to the ultra-high vacuum (UHV) chamber. In this configuration, the beam current, specific to a given ion energy, can be finely adjusted based on magnetron power, working pressure, and extraction voltage. Consequently, optimizing the dependence of beam current on these parameters is a worthwhile pursuit, driven by the need to comprehend the underlying scientific principles. Additionally, the ion current (beam current) is influenced by the extracted ion energy and the position of the target. Hence, a comprehensive investigation into the intricate relationship between ion current and the mentioned parameters emerges as a compelling topic in the current scientific context.

Optimization of ion current on various plasma parameters:

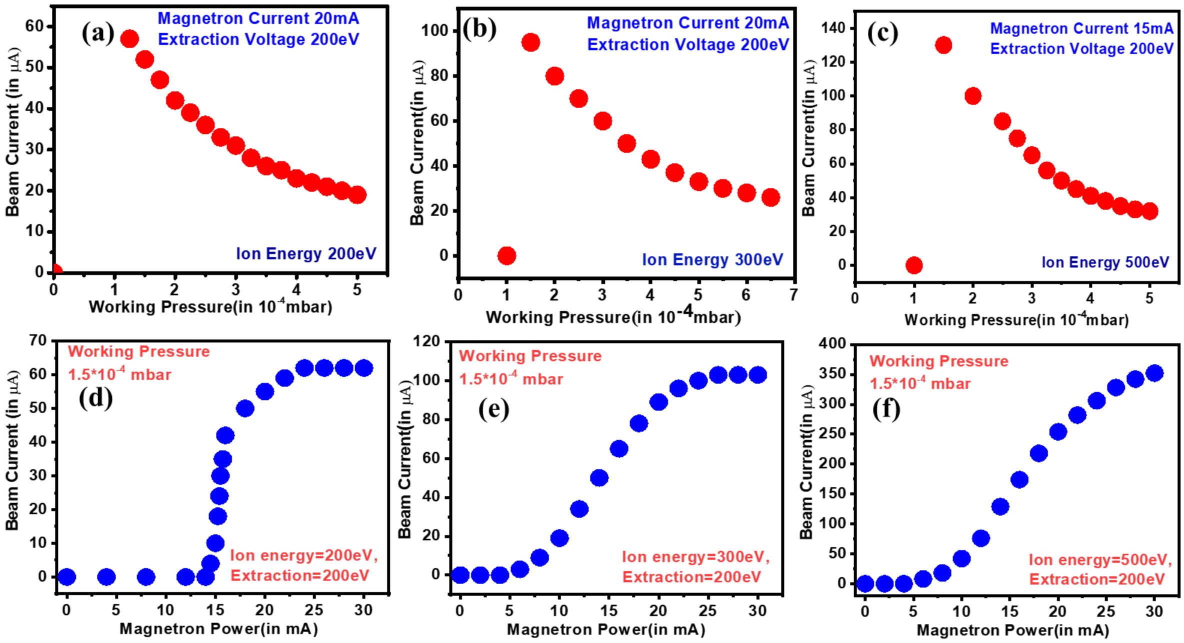

Figure 3: Variation of beam current with (a)–(c) plasma pressure, (d)–(f) microwave (magnetron) power for different ion energy.

The variation of beam current with plasma pressure and magnetron (microwave) power for different ion energies are investigated and presented in Figure 3. Figure 3(a)-(c) demonstrates that the beam current decays almost exponentially with the increase in plasma pressure. The ion current is maximum at plasma pressure 1.5×10^{-4} mbar irrespective of ion energies. This indicates that the minimum base pressure required for generating plasma is 1.5×10^{-4} mbar. It is also evident that for the same plasma pressure, the beam current is maximum for the highest ion energy. The gas pressure inside the plasma cup is directly proportional to the number of gas molecules present. At low plasma pressure, the mean free path of gas molecules is larger due to the lesser density of gas molecules, which allows the produced ions to traverse a longer distance without collision. This increases the ionization efficiency, and hence, with fewer no of collisions, the probability for recombination of the ions is very low. Consequently, a large number of ions are extracted, intensifying the beam current. The entire phenomenon can be summarised through the equation, $\lambda = (\sigma.n)^{-1}$, where λ is the mean free path of the ions, σ is the cross section for recombination, and n is the density of the ions inside the plasma [25–27]. The mean free path of the ions, determined by the recombination cross section and density of plasma, plays a key role in quantifying the ion current.

Further, the conversion of the gas to plasma is governed by a magnetron (microwave) source and therefore, the ion current or plasma density must depend on magnetron power. To understand that, the variation of ion current with microwave power is recorded at different plasma pressures and ion energies, as presented in Figure 3 (d)- (f). In general, the plasma density (n) depends on the microwave frequency (ω) as $n = \frac{E_{RF}\omega^2}{\varepsilon}$ where E_{RF} is the microwave power (energy) and ε is the minimum energy required for ion-electron pair generation [25]. The magnitude of ε is different for different gases. A non-zero magnitude of ε signifies the minimum energy needed to generate plasma, commonly referred to as ionization energy, which is supplied by magnetron power. It is evident from the above Figure (3(d)-(e)) that up to the microwave power equal to a critical value, the formation of plasma is forbidden, resulting in a zero-beam current. With the increase of magnetron power beyond the magnitude ε, the beam current increases almost linearly with the input magnetron power, since the plasma density (n) is directly proportional to the microwave power (E_{RF}). The beam current reaches saturation at a specific microwave power level, which varies based on the ion energy. At sufficiently high microwave power, the plasma density (beam current) is high, and the rate of generation and recombination of the ion-electron pair is equal, resulting in a saturation of beam current as observed in Figure. 3(d)-(f). Further, the cut off power also depends on ion energy. At sufficiently low ion energy, the microwave power required for generating plasma is high. With higher ion energies microwave power required for ion-electron pair generation is also less which is obvious from the above discussion.

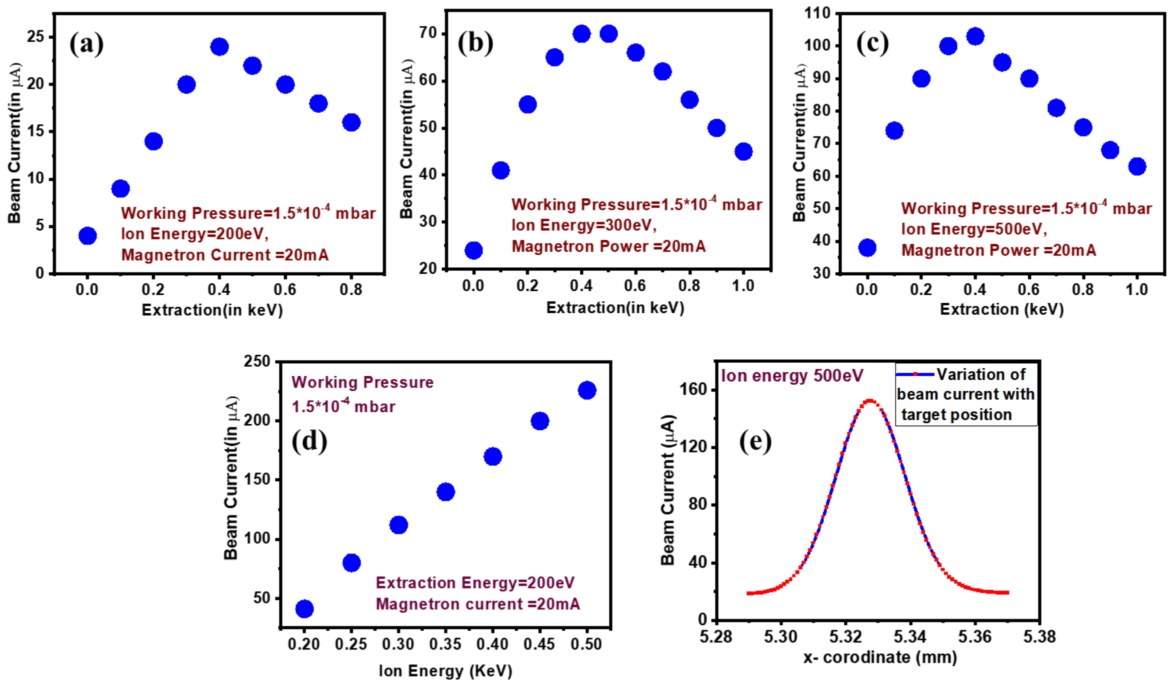

Figure 4: Variation of (a)-(c) beam current with ion extraction voltage at different ion energy;(d) beam current with ion energy; (e) beam current with the target position.

The extraction of developed Ar-ion beam was governed by a combination of three-grid (concave) ion optics system [28–30]. The beam current and the beam profile depend on the potential applied at the grid and the target position. The change in beam current with the ion extraction voltage recorded for different ion energies is presented in Figure. 4 (a)-(c). Initially, the beam current increases linearly with the applied extraction voltage since more ions are extracted with a higher extraction voltage. Irrespective of ion energy, the beam current is a maximum extraction voltage of 200 eV. With further increases in extraction voltage, the beam current decreases rapidly. This is governed by two major phenomena, firstly, the space charge effect, i.e., a high extraction voltage, creates an electrostatic field that repels the subsequent ions, causing the beam to spread out; therefore, the current density reduces. Secondly, during the extraction of the ions, the application of a high extraction voltage leads to the collision of the ions with residual gas molecules, which also causes a significant decrease in beam current due to ion-electron recombination. Generally, the extraction voltage is kept fixed to maintain the shape of the beam, essential for uniform irradiation of samples.

The dependence of beam current upon ion energy is also investigated in Figure 4(d). It is clear from Figure 4(d) that the beam current increases almost linearly with the increase in ion energy at a fixed extraction voltage and microwave power. When the applied extraction voltage is 200 eV and the ion energy is less than 200 eV, then the number of ions that can overcome the barrier of 200 eV is less, causing a low beam current. With the increase in ion energy, the ions achieve sufficient energy to overcome the barrier of 200 eV; hence, the beam current increases. On the other hand, for a particular ion energy, lowering the extraction voltage also results to a lowering of beam current as observed from the above Figure 4 (a)-(c). Therefore, to maintain a proper beam shape and adequate beam current, the extraction voltage and ion energy are to be precisely optimized. Further, the variation of beam current with the target position, known as the beam profile, is also presented in Figure 4(e). The beam profile is Gaussian in nature for concave grid (molybdenum) beam extraction optics. Such a beam profile precisely ensures the target position is for maximum beam current.

Nano-structuring on Si surface by 450 eV Ar-ion bombardment:

Subsequently, after a detailed optimization of the ultra-low energy Ar-ion beam, the surface topography of Si (investigated by AFM) after the off-normal bombardment of 450 eV Ar-ion at different incidence angles and time is investigated. Figure 5 represents the surface morphology of Si surface after 450 eV Ar-ion bombardment at different incidence angles. The arrow on the right-hand side indicates the direction of the ion beam concerning the surface normal. The irradiation of silicon surface with 450 eV Ar-ion at an angle of 55º leads to no development of surface morphology, and presented in Figure 5(a). However, at an ion incidence angle of 58º, the evolution of surface morphology starts, although no prominent ripple structure is observed (Figure 5(b)). On the other hand, the bombardment of 450 eV Ar-ion on the Si surface for an hour at an angle of 60º concerning surface normal leads to the formation of a well-defined nanoscale ripple pattern as observed in Figure 5(c). The growth of the ripple becomes more prominent with the increase in bombardment time. The amplitude of the ripple grows larger with longer bombardments of Ar-ions.

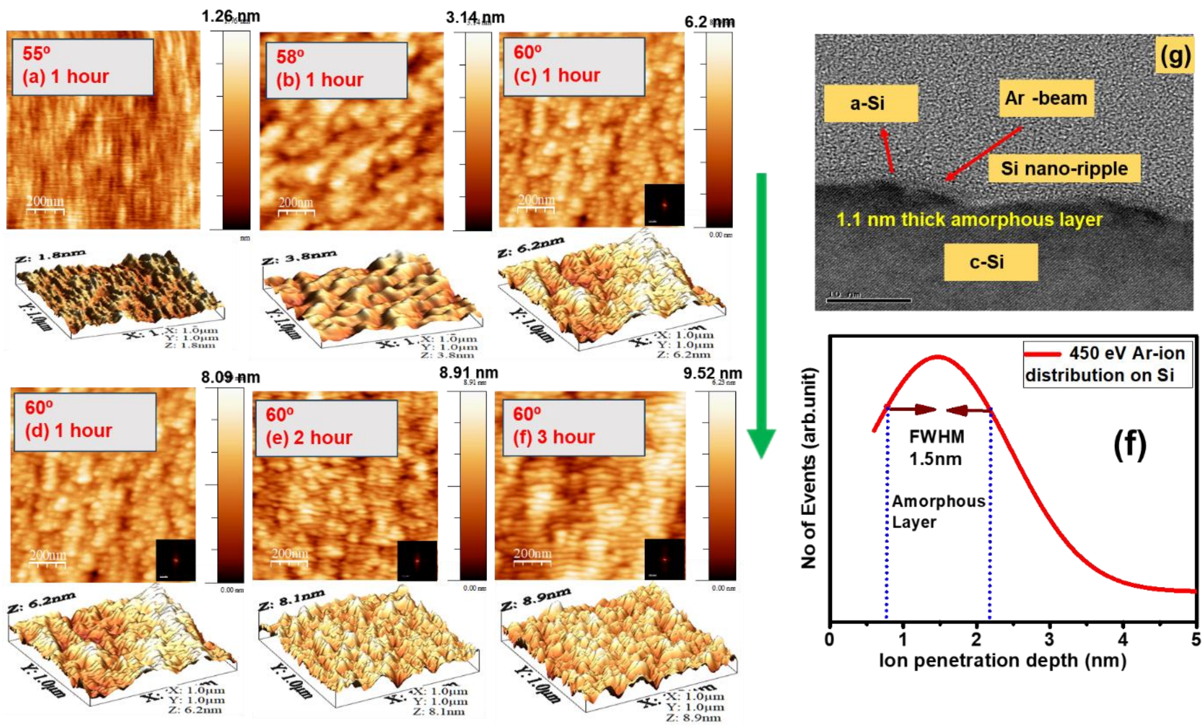

Figure 5: AFM image (2D and 3D) of the evolution of surface morphology by 450 eV Ar-ion bombarded at different incidence angles and time. The arrow indicates the ion beam direction.

To visualize the growth of the ripple, the 3D AFM images are presented along with the 2D images. It is clear from the height scale associated with the images, that the ripple height increases with bombardment time. The first Fourier transform (FFT) image of nano-patterned surface is inset at the right lowest corner of each image. In the present case, the fluence is replaced by irradiation time. The quality and the growth of the nano-structures are quantitatively discussed in Figure 6, where a detailed variation of ripple wavelength, rms roughness, and the power spectral density is discussed.

Figure 5(g) represents the cross-sectional transmission electron microscopy (TEM) image of 450 eV Ar-ion bombarded Si surface at an angle of 60º with a time of 3 hours. The presence of Ar-ion-induced surface corrugation in terms of ripple-like nanostructure is evidenced in Figure. 5(g). Although the amplitude of the ripples is not sufficiently large, the observed ripple wavelength of around 31 nm from the TEM image, is consistent with that of AFM data (presented in Figure 6(e)). However, in addition to the ripple-like nanostructure, an ultra-thin amorphous layer formation occurs due to Ar-ion bombardment. The thickness of the amorphous layer is around 1.5 nm, which is consistent with the penetration depth of the Ar-ions (1.2 nm), estimated by Monte Carlo Simulation (Fig 5(f)) [24]. Therefore, the topographical image is consistent with the cross-sectional image, indicating a clear signature of ripple-like nano-structure formation.

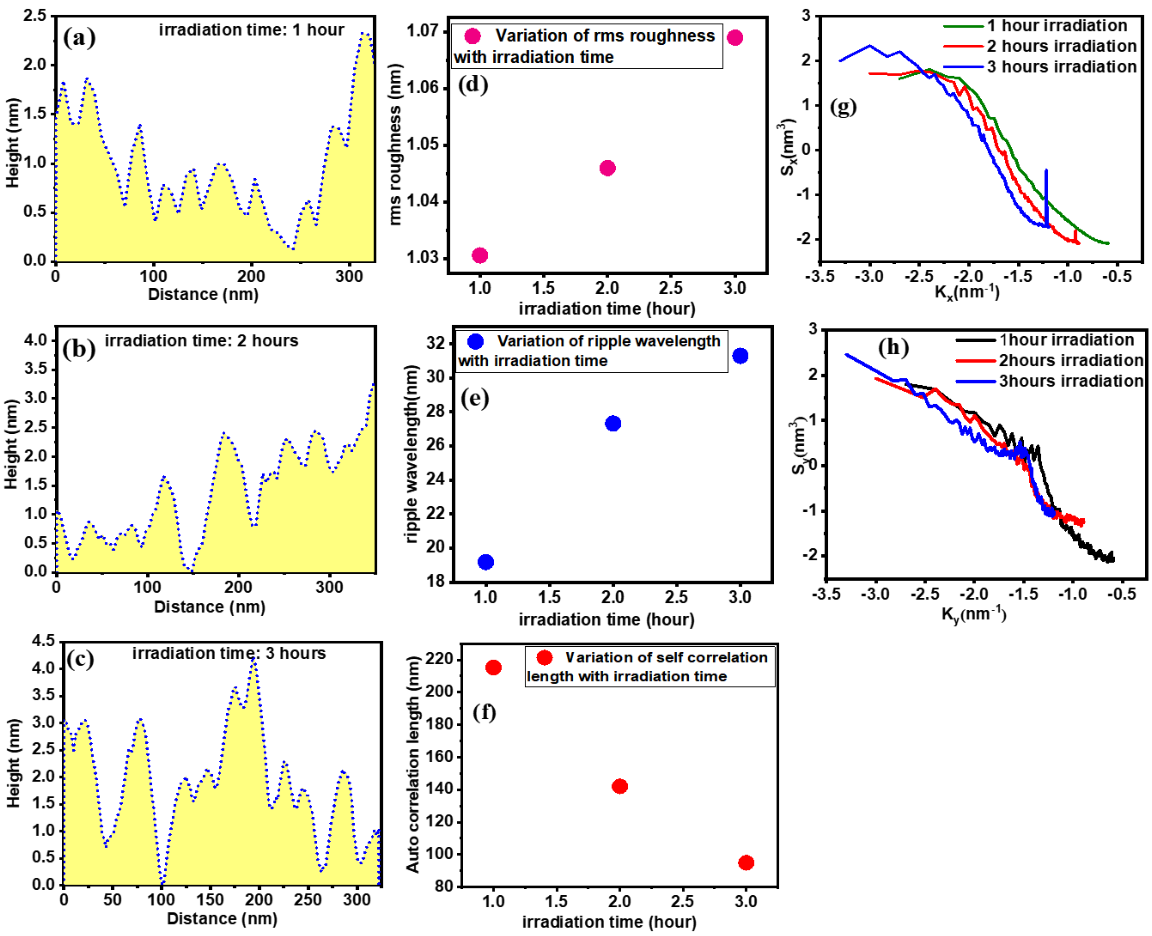

Figure 6: Variation of (a) – (c) surface height modulation of nano-patterned silicon surface; (d) ripple wavelength and (e) rms roughness with irradiation time. Variation of power spectral density of nanopatterned silicon surface on (g) parallel and (h) perpendicular direction.

Figure 6 (a)-(c) indicate the variation of the surface profile of the nano-patterned AFM images shown in Figure 5. The height profile is the direct evidence of variation of ripple amplitude with irradiation time. The increase in ripple height with irradiation time is shown in Figure 6 (a)-(c). Further, the fluctuation in ripple height or amplitude generally termed rms roughness, is also investigated in Figure 6(d). It is clear from Figure 6(d), that rms roughness increases linearly with the irradiation time (fluence). Further, the ordering of the nanostructure with the bombardment time, examined in terms of ripple wavelength, is presented in Figure 6(e). From Figure 6(e) initially, the ripple wavelength increases as the bombardment time increases from one hour to two hours. With a further increment in irradiation time, the change of ripple wavelength is negligible, i.e., a saturation of ripple wavelength is observed. The degree of similarity between two spatial morphologies is generally quantified by auto-correlation length or self-correlation length, as presented in Figure 6(f). It is clear from Figure 6(f), that the auto-correlation length decreases with bombardment time. This indicates a more ordered ripple structure is found to develop with higher irradiation time. To understand the growth of the ripple structure, the power spectral density factor along the parallel and perpendicular direction of the developed ripple is presented in Figure 6 (g)-(h). The prominent peak present in Figure 6(g) indicates, the development of ripple structure along the x direction (parallel) with a particular wavevector (k_x). Besides, the absence of a ripple wavevector in perpendicular mode is evidenced in Figure 6(h). Therefore, 450 eV Ar-ion bombardment on Si, leads to well-defined parallel mode ripple formation at off-normal incidence.

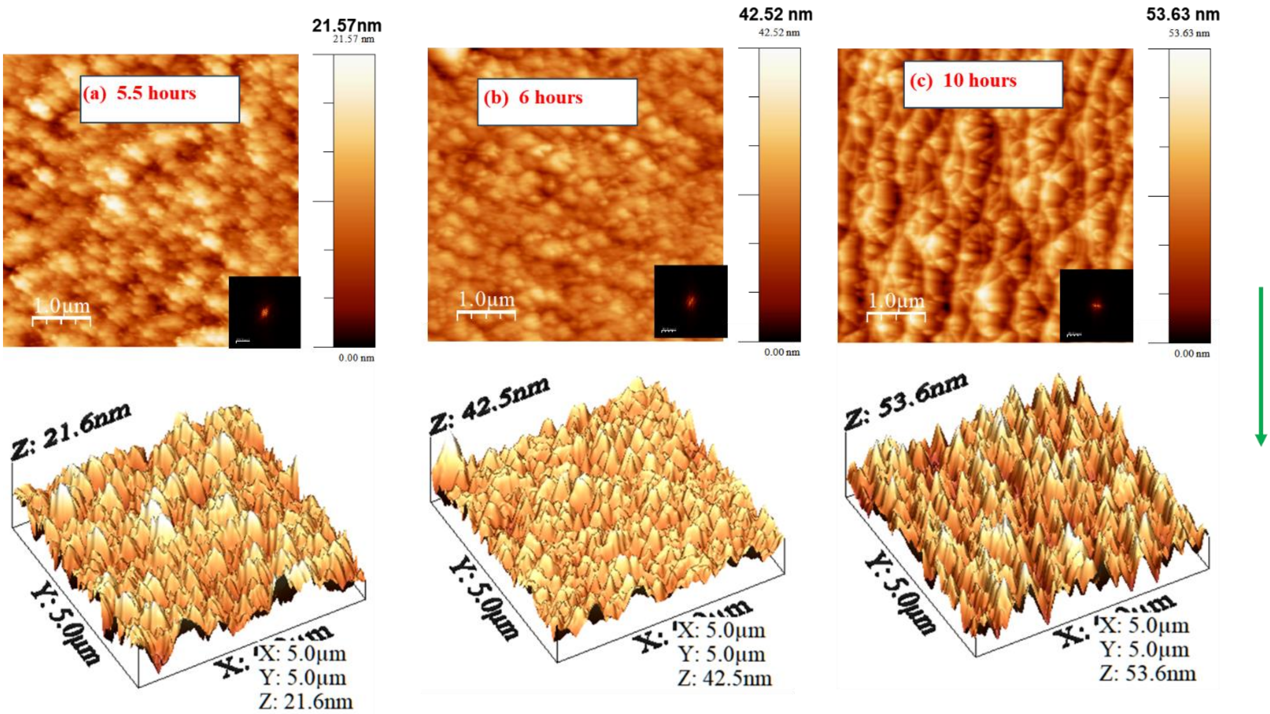

Figures 7: AFM images (2D and 3D) of the evolution of nano-structure on Si surface with time under 450 eV Ar-ion bombardment at an angle of 72.5º.

Figure 7 illustrates the surface topography after 450 eV Ar-ion bombarded the silicon surface at an angle of 72.5º with different bombardment time. Corresponding 3D AFM images are also presented along with 2D surface topography. Generally, the transformation of well-defined nano ripples into nano-facets occurs at this near-grazing angular region[31]. In the present case, although no prominent nano-facet formation is observed, a clear signature of transformation of ripple structure towards nano-facets is seen. At sufficiently large bombardment time (10 hours), nano-facets like structures with larger dimensions are developed, although the facets are not well organized. It is also evident that the rms roughness is also increasing with bombardment time.

Surface nano-structuring by energetic ion bombardment is a consequence of ion-beam-induced off-normal (60º and 72.5º) sputtering of surface atoms and their consecutive redistribution [9,32,33]. During ion bombardment, the unequal radius of curvature of the surface ensures unequal deposition of energy at different points on the surface, which results in unequal sputtering at those points. This generates surface instability, and consequently, the surface atoms are redistributed to stabilize the surface. These two effects jointly trigger nano-pattern formation on the surface. A first theoretical model was proposed by Bradley and Harper [34], based on curvature-dependent sputtering of surface and near-surface atoms. Later, Carter and Vishnyakov introduced the concept of redistribution of surface atoms [35]. In present days, several experiments have been carried out to understand other factors that contribute to nano-pattern formation, such as preferential and differential sputtering, the role of surface and beam impurities, the effect of chemical compound formation, and compound ion irradiation. In cases of ultra-low energy ion bombardment, the rate of sputtering is lower compared to medium-energy ion bombardment; therefore, in this case, mass redistribution of the surface atoms plays a key role. Being inert, the reaction between Ar-ion and Si atoms is forbidden, ensuring the absence of the chemical aspect of pattern formation. However, the native silicon oxide layer partially sputters out with the bombardment of Ar-ion. In the present case, the sputtering of elemental Si atoms takes place along with the Si atoms in oxide form. This is also a key factor in generating surface instability. The surface morphology largely varies due to different amounts of near-surface mass transport by the surface-confined ion-enhanced viscous flow[36]. Here in the present case, up to an ion incidence angle of 58º, the surface remains unstable under 450 eV Ar-ion bombardment. Due to such sputtering, a well-defined ripple formation is found after an hour of 450 eV Ar-ion bombardment. With the increase in bombardment time, Si atoms in both elemental and oxide form sputter more, and a well-ordered ripple is obtained. However, due to the presence of the ripple, the surface becomes anisotropic. The consequence of such an anisotropic nature of the surface is investigated and discussed in the upcoming section.

Application of nano-patterned Si surface:

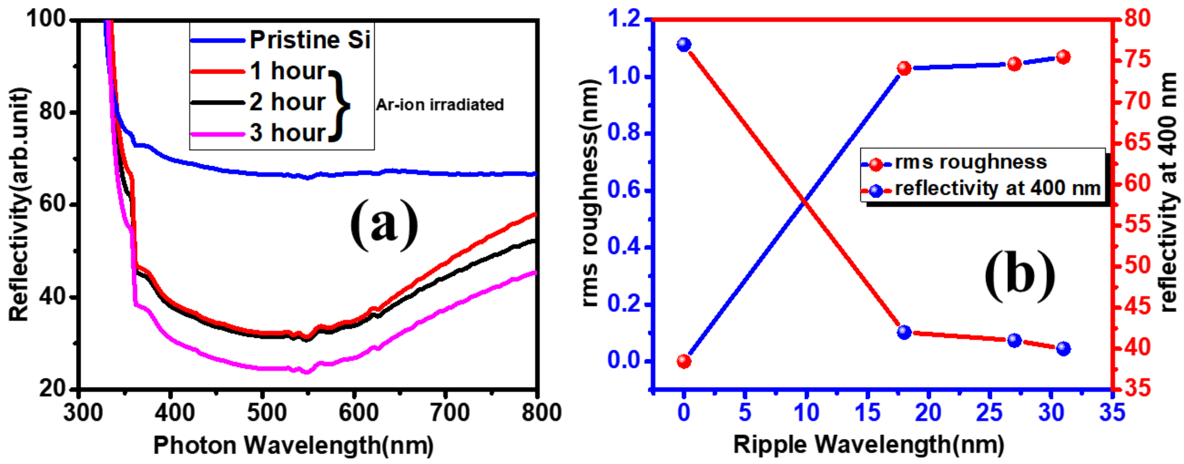

Figure 8: (a) UV-VIS-IR spectra of pristine and nano-patterned surfaces, (b) variation of rms roughness and reflectivity with ripple wavelength.

The optical response of pristine and Ar-ion-induced nano-patterned silicon surfaces are investigated through UV-VIS reflectivity & presented in Figure 8. Figure 8(a) depicts the change in reflectivity of the silicon surface due to the presence of nano-pattern. With the increase of bombardment time, reflectivity decreases drastically. Further the change in reflectivity in UV region with respect to rms roughness and ripple wavelength is also investigated in Fig 8(b). It is clear from the Fig 8(b), that the reflectivity decreases with the increase in ripple wavelength. Further, variation of the rms roughness of the Ar-ion irradiated nano-patterned Si surfaces is nominal. In general, the presence of nano-patterns on the surface enhances the reflection of UV-VIS light, due to light trapping by multiple reflections [37–39]. The presence of a well-defined ripple pattern, formed due to Ar-ion bombardment (for three hours), leads to the development of a well-defined nanopattern on the silicon surface and hence the reflectivity is minimal compared to the other two surfaces. The change in reflectivity depends on the change in the electronic structure as well as surface topography of the material. Such a change in electronic structure can contain several factors, like the change in chemical nature or impurity incorporation on the surface, and amorphization of the surface. Ar-being inert causes no chemical modification of the silicon surface, along with the absence of the trapped Ar-ion on silicon surface (concluded from TEM image in Fig 5(g)), particularly in this lower energy regime. Therefore, in the present case, the amorphization due to ion beam sputtering, the amorphization of the silicon surface, and the nanostructure formation on the surface, together change the electronic density of the material, causing a lowering in reflectivity. The tailoring of the reflectivity by developing nano-structure is widely applicable for anti-reflective (ARC) coating and photovoltaic device applications [40,41].

The formation of nano-structure on the silicon surface by inert ion bombardment is a consequence of ion-induced instability on the surface by the interplay between sputtering and mass redistribution of surface atoms [42,43]. During ion bombardment, the sputtering of the native silicon oxide layer along with the bulk silicon takes place. The rate of sputtering of silicon oxide and the elemental silicon is different which initiates the instability at the initial time of bombardment. Further, the instability is enhanced by differences in the sputtering yield of silicon in native oxide and elemental form. These two effects are jointly responsible for developing the nano-pattern on the surface. With the increasing bombardment time, the rate of sputtering of Si in elemental and compound form increases, and a well-defined periodic structure is observed. Further, during sputter erosion, the native oxide layer is mostly removed, forming a silicon ripple structure. Further, the exposure of the nano-patterned silicon surface to air during optical measurement ensures the formation of non-uniform silicon oxide on the nano-patterned silicon surface. Due to such preferential spatial formation of silicon oxide, the change in reflectivity is triggered. Therefore, nano-patterned silicon surfaces can be an alternative for memory devices.

Conclusion:

In this comprehensive study, the intricacies of an ultra-low energy magnetron-based Electron Cyclotron Resonance (ECR) ion source are studied systematically by exploring optimal parameters to achieve stable and intense beam currents. The cost-effectiveness and versatility of this ion source make it particularly noteworthy, offering a practical solution for generating reasonable beam currents. Notably, the ion source operates within an ultra-high vacuum environment, rendering it valuable for both implantation and deposition processes. Our meticulous investigation into the ECR-based ultra-low energy ion source lays the groundwork for ion beam-induced nano-structuring and layer-wise material modification, affording precise control over ion penetration depth and fluence. The manuscript emphasizes an intriguing alternative perspective by highlighting the in-depth optimization of low energy ion source and inert ion-induced nano-patterning as a viable approach for ARC coating. Additionally, the manuscript underscores the potential of nano-patterned silicon surfaces as an alternative material for tailoring reflectivity, particularly for Anti-Reflective Coating (ARC) applications. This study not only advances our understanding of ECR-based ion sources but also opens avenues for innovative applications in nanotechnology and materials science.

Acknowledgement:

The authors thank the Department of Atomic Energy, Govt. of India for financial support.

References:

(1) Bhowmick, S.; Mukherjee, J.; Satpati, B.; Karmakar, P. *Appl Surf Sci* **2022**, *578*. doi:10.1016/j.apsusc.2021.152079

(2) Barofsky, D. F. *Mass Spectrometric Analyses in Agriculture and Natural Product Research*; 1999; Vol. 29

(3) Gambino, N.; Myalsky, S.; Adler, L.; De Franco, A.; Ecker, F.; Guidoboni, G.; Kurfürst, C.; Penescu, L.; Pivi, M.; Schmitzer, C.; Strasik, I.; Wastl, A. Impact of Ion Source Stability for a Medical Accelerator. In *Journal of Instrumentation*; Institute of Physics Publishing, 2019; Vol. 14. doi:10.1088/1748-0221/14/05/C05017

(4) Gammino, S. Ion Sources for Medical Applications. In *CERN Yellow Reports: School Proceedings*; CERN, 2017; Vol. 1, pp 59–70. doi:10.23730/CYRSP-2017-001.59

(5) Satoh, K.; Oono, Y. Studies on Application of Ion Beam Breeding to Industrial Microorganisms at Tiara. *Quantum Beam Science*. MDPI June 1, 2019. doi:10.3390/qubs3020011

(6) Mukherjee, J.; Bhowmik, D.; Mukherjee, M.; Satpati, B.; Karmakar, P. *J Appl Phys* **2020**, *127*. doi:10.1063/1.5144960

(7) Mukherjee, J.; Bhowmik, D.; Bhattacharyya, G.; Satpati, B.; Karmakar, P. *Journal of Physics Condensed Matter* **2022**, *34*. doi:10.1088/1361-648X/ac4937

(8) De Lima, L. H.; Cun, H. Y.; Hemmi, A.; Kälin, T.; Greber, T. Note: An Ion Source for Alkali Metal Implantation beneath Graphene and Hexagonal Boron Nitride Monolayers on Transition Metals. In *Review of Scientific Instruments*; 2013; Vol. 84. doi:10.1063/1.4848936

(9) Norris, S. A.; Aziz, M. J. Ion-Induced Nanopatterning of Silicon: Toward a Predictive Model. *Applied Physics Reviews*. American Institute of Physics Inc. March 1, 2019. doi:10.1063/1.5043438

(10) Teshome, B.; Facsko, S.; Keller, A. *Nanoscale* **2014**, *6*, 1790–1796. doi:10.1039/c3nr04627c

(11) Bhowmik, D.; Karmakar, P. *Surf Coat Technol* **2020**, *385*. doi:10.1016/j.surfcoat.2020.125369

(12) Mollick, S. A.; Singh, R.; Kumar, M.; Bhattacharyya, S.; Som, T. *Nanotechnology* **2018**, *29*. doi:10.1088/1361-6528/aaaa74

(13) Parida, B. K.; Kundu, A.; Hazra, K. S.; Sarkar, S. *Appl Phys A Mater Sci Process* **2021**, *127*. doi:10.1007/s00339-021-05117-0

(14) Bhowmick, S.; Mukherjee, J.; Satpati, B.; Karmakar, P. *Appl Surf Sci* **2022**, *578*. doi:10.1016/j.apsusc.2021.152079

(15) Kasani, S.; Curtin, K.; Wu, N. A Review of 2D and 3D Plasmonic Nanostructure Array Patterns: Fabrication, Light Management and Sensing Applications. *Nanophotonics*. De Gruyter 2019. doi:10.1515/nanoph-2019-0158

(16) Saini, M.; Singh, R.; Sooraj, K. P.; Basu, T.; Roy, A.; Satpati, B.; Srivastava, S. K.; Ranjan, M.; Som, T. *J Mater Chem C Mater* **2020**, *8*, 16880–16895. doi:10.1039/d0tc03862h

(17) Abdel Rahman, M. M.; Abdel Salam, F. W.; Soliman, B. A. Improved Treatment of Home-Made Glow Discharge Ion Source. In *Journal of Physics: Conference Series*; Institute of Physics, 2022; Vol. 2304. doi:10.1088/1742-6596/2304/1/012011

(18) Publications, T. J. G.; Gaus, A. D.; Htwe, W. T.; Brand, J. A.; Gay, T. J.; Schulz, M.; Gay, T. J. *DigitalCommons@University of Nebraska-Lincoln DigitalCommons@University of Nebraska-Lincoln Energy Spread and Ion Current Measurements of Several Ion Energy Spread and Ion Current Measurements of Several Ion Sources Sources Energy Spread and Ion Current Measurements of Several Ion Sources*; 1994

(19) Schmor, P. W. *A REVIEW OF POLARIZED ION SOURCES*; 1996

(20) Angra, S. K.; Kumar, P.; Dongaonkar, R. R.; Bajpai, R. P. *Unstable Plasma Characteristics in Mirror Field Electron Cyclotron Resonance Microwave Ion Source*; 2000; Vol. 54

(21) Asmussen, J. *Journal of Vacuum Science & Technology A: Vacuum, Surfaces, and Films* **1989**, *7*, 883–893. doi:10.1116/1.575815

(22) Schmidt, A. A.; Offermann, J.; Anton, R. *Thin Solid Films* **1996**, *281–282*, 105–107. doi:10.1016/0040-6090(96)08586-0

(23) Anton, R.; Wiegner, T.; Naumann, W.; Liebmann, M.; Klein, C.; Bradley, C. *Review of Scientific Instruments* **2000**, *71*, 1177–1180. doi:10.1063/1.1150420

(24) Ziegler, J. F.; Ziegler, M. D.; Biersack, J. P. *Nucl Instrum Methods Phys Res B* **2010**, *268*, 1818–1823. doi:10.1016/j.nimb.2010.02.091

(25) Ohtsu, Y. Physics of High-Density Radio Frequency Capacitively Coupled Plasma with Various Electrodes and Its Applications. In *Plasma Science and Technology - Basic Fundamentals and Modern Applications*; IntechOpen, 2019. doi:10.5772/intechopen.78387

(26) Chu, P. K.; Qin, S.; Chan, C.; Cheung, N. W.; Ko, P. K. *IEEE Transactions on Plasma Science* **1998**, *26*, 79–84. doi:10.1109/27.659535

(27) Ghosh, S. N.; Dhungel, S. K.; Yoo, J.; Gowtham, M.; Yi, J.; Bora, D. *Study of High-Density Helicon-Plasma Generation and Measurement of the Plasma Parameters by Using a Frequency-Compensated Langmuir Probe*; 2006; Vol. 48

(28) Yang, Y. R.; Fu, S. H.; Ding, Z. F. *AIP Adv* **2022**, *12*. doi:10.1063/5.0082813

(29) Fournier, P.; Lisi, N.; Meyer, C.; Scrivens Cern, R.; Division, P. S.; Ostroumov, P. *Experimental Characterisation of Gridded Electrostatic Lens (GEL) Low Energy Beam Transport (LEBT) for the Laser Ion Source (LIS) and Effect of a Wire Grid on the Extraction Electrode*; 1999

(30) Dudin, S. V.; Rafalskyi, D. V. *European Physical Journal D* **2011**, *65*, 475–479. doi:10.1140/epjd/e2011-20402-y

(31) Deka, A.; Barman, P.; Mukhopadhyay, M. K.; Bhattacharyya, S. R. *Surfaces and Interfaces* **2021**, *25*. doi:10.1016/j.surfin.2021.101242

(32) Jain, I. P.; Agarwal, G. Ion Beam Induced Surface and Interface Engineering. *Surface Science Reports*. Elsevier B.V. 2011, pp 77–172. doi:10.1016/j.surfrep.2010.11.001

(33) Datta, D. P.; Garg, S. K.; Basu, T.; Satpati, B.; Hofsäss, H.; Kanjilal, D.; Som, T. *Appl Surf Sci* **2016**, *360*, 131–142. doi:10.1016/j.apsusc.2015.10.133

(34) Bradley, R. M.; Harper, J. M. E. *Journal of Vacuum Science & Technology A: Vacuum, Surfaces, and Films* **1988**, *6*, 2390–2395. doi:10.1116/1.575561

(35) Carter, G.; Vishnyakov, V. *Roughening and Ripple Instabilities on Ion-Bombarded Si*; 1996

(36) Vorathamrong, S.; Panyakeow, S.; Ratanathammaphan, S.; Praserthdam, P. *AIP Adv* **2019**, *9*. doi:10.1063/1.5084344

(37) Mennucci, C.; Muhammad, M. H.; Hameed, M. F. O.; Mohamed, S. A.; Abdelkhalik, M. S.; Obayya, S. S. A.; Buatier de Mongeot, F. *Appl Surf Sci* **2018**, *446*, 74–82. doi:10.1016/j.apsusc.2018.02.186

(38) Garnett, E.; Yang, P. *Nano Lett* **2010**, *10*, 1082–1087. doi:10.1021/nl100161z

(39) Amalathas, A. P.; Alkaisi, M. M. Nanostructures for Light Trapping in Thin Film Solar Cells. *Micromachines*. MDPI AG September 1, 2019. doi:10.3390/mi10090619

(40) Mousavi, B. K.; Mousavu, A. K.; Busani, T.; Zadeh, M. H.; Brueck, S. R. J. *Journal of Applied Mathematics and Physics* **2019**, *07*, 3083–3100. doi:10.4236/jamp.2019.712217

(41) Zang, K.; Jiang, X.; Huo, Y.; Ding, X.; Morea, M.; Chen, X.; Lu, C. Y.; Ma, J.; Zhou, M.; Xia, Z.; Yu, Z.; Kamins, T. I.; Zhang, Q.; Harris, J. S. *Nat Commun* **2017**, *8*. doi:10.1038/s41467-017-00733-y

(42) Madi, C. S.; Anzenberg, E.; Ludwig, K. F.; Aziz, M. J. *Phys Rev Lett* **2011**, *106*. doi:10.1103/PhysRevLett.106.066101

(43) Chan, W. L.; Chason, E. *J Appl Phys* **2007**, *101*. doi:10.1063/1.2749198